Wind Sea Growth and Dissipation in the Open Ocean

JEFFREY L. HANSON

The Johns Hopkins University Applied Physics Laboratory, Laurel, Maryland

OWEN M. PHILLIPS

The Johns Hopkins University, Baltimore, Maryland

(Manuscript received 12 December 1997, in final form 17 June 1998)

ABSTRACT

Wind sea growth and dissipation in a swell-dominated, open ocean environment is investigated to explore the use of wave parameters in air–sea process modeling. Wind, wave, and whitecap observations are used from the Gulf of Alaska surface scatter and air–sea interaction experiment (Critical Sea Test-7, Phase 2), conducted 24 February through 1 March 1992. Wind sea components are extracted from buoy directional wave spectra using an inverted catchment area approach for peak isolation with both wave age criteria and an equilibrium range threshold used to classify the wind sea spectral domain. Dimensionless wind sea energy is found to scale with inverse wave age independently of swell. However, wind trend causes significant variations, such as underdeveloped seas during rising winds. These important effects are neglected in wind-forced air–sea process models.

The total rate of wave energy dissipation is conveniently estimated using concepts from the Phillips equilibrium range theory. Replacing wind speed with wave dissipation rate in the standard power-law description of oceanic whitecap fraction decreases the range of data scatter by two to three orders of magnitude. The improved modeling of whitecaps demonstrates that wave spectral parameters can be used to enhance air–sea process models.

1. Introduction

The detailed physical mechanisms by which wind waves grow and evolve remain an intriguing unsolved mystery of fluid mechanics. Most field observations of wind wave growth characteristics have been made in well-defined geometrical scenarios with steady prevailing winds, well-understood fetch, and no swell. An analysis of fully developed wind seas by Pierson and Moskowitz (1964) verified earlier theoretical notions that there is a universal similarity in spectral shape (Kitaigorodskii 1962) with an asymptotic upper bound (Phillips 1958). However, a peak enhancement effect observed during the Joint North Sea Wave Project (JONSWAP) was found to have no correlation with various fetch relationships (Hasselmann et al. 1973). In a study of fetch-limited waves on Lake Ontario, Donelan et al. (1985) noted that the peak enhancement depends on inverse wave age U_c/c_p, where U_c is the component of the 10-m-elevation wind speed (U_{10}) in the mean direction of the waves at the spectral peak, and c_p is the wave phase speed. To further refine the wave fetch relationships, Donelan et al. (1992) made extensive wind and wave measurements on Lake St. Clair out to a fetch of approximately 21 km. They note a very high degree of correlation of nondimensional wind sea energy $e' = eg^2/U_c^4$ with U_c/c_p, where the total energy (variance) is defined by integrating the directional wave spectrum $S(\omega, \theta)$ over frequency (ω) and direction (θ):

$$e = \int_\omega \int_\theta S(\omega, \theta)\, d\omega\, d\theta.$$

The effect of swell on wind wave growth has been a topic of active research for many years with inconsistent results. Selected findings are summarized in Table 1. Although numerous well-documented experiments show unequivocally that short laboratory wind waves exhibit reduced amplitudes when in the presence of longer paddle-generated waves, the details are often contradictory among investigations. Furthermore, there remain a variety of competing theories to explain these phenomena. Most surprising, perhaps, is that modification of wind-driven gravity waves by swell has yet to be demonstrated in the real ocean. This is partially due to the difficulties of separating naturally observed wind sea from swell. Note that only a single study from Table 1 was conducted in oceanic conditions (Dobson et al. 1988). In a fetch-limited coastal environment, Dobson and colleagues do not report any significant

Corresponding author address: Dr. Jeffrey L. Hanson, Applied Physics Laboratory, The Johns Hopkins University, Johns Hopkins Road, Laurel, MD 20723.
E-mail: jeffrey.hanson@jhuapl.edu

TABLE 1. The modification of wind waves by swell: selected results.

Reference	Investigation	Relevant conclusions
Cox (1958)	Laboratory	Short wave mean square slope is highest just ahead of long wave peaks.
Longuet-Higgins and Stewart (1960)	Theoretical	Short waves become shorter and steeper at the crest of superposed long waves owing to radiation stress interactions.
Mitsuyasu (1966)	Laboratory	Wind wave energy attenuation depends on steepness of aligned swell waves.
Phillips and Banner (1974)	Laboratory/ theoretical	Enhanced short wave breaking near long wave crests results from intensified drift of aligned and opposed swell.
Wright (1976); Plant and Wright (1977)	Laboratory/ theoretical	Drift-enhanced dissipation theory does not agree with observations.
Hatori et al. (1981)	Laboratory	An unidentified nonlinear process transfers energy from wind waves to superposed long waves.
Donelan (1987)	Laboratory	Energy input by wind is unaffected by superposed long waves. Resonant nonlinear interaction ''detuning'' may cause wind wave energy loss.
Dobson et al. (1988)	Field	Fetch-limited wind sea growth is not influenced by opposed swell.
Smith (1990)	Theoretical	Physical model including drift-enhanced dissipation roughly agrees with observations.
Mitsuyasu (1992)	Laboratory	Wind sea is intensified by opposed swell.
Chu et al. (1992)	Laboratory	Wind seas are shortened and attenuated by aligned swell; wind sea slope remains nearly constant.

growth effects resulting from the presence of an opposing swell. They present results that are statistically identical to the Lake Ontario results of Donelan et al. (1985). They attribute this similarity to the short fetches involved with both studies.

Breaking surface waves are observed on any open body of water over which the wind exceeds approximately 3 m s^{-1}. In a recent review, Melville (1996) notes that breaking waves contribute to wave evolution by effectively dissipating excess energy originally input by the wind. The importance of this role is evidenced in the radiative transfer equation, which describes the conservation of wave action spectral density $N(\mathbf{k}) = gS(\mathbf{k})/\omega$ of waves interacting with a current of velocity $\mathbf{U}$ (Phillips 1977; Komen et al. 1994) in wave number ($\mathbf{k}$) space:

$$\frac{dN}{dt} = \frac{\partial N}{\partial t} + (\mathbf{c}_g + \mathbf{U}) \cdot \nabla N = -\nabla_k \cdot \mathbf{T}(\mathbf{k}) + S_w - D, \quad (1)$$

where $\mathbf{c}_g$ is the wave group velocity; $-\nabla_k \cdot \mathbf{T}(\mathbf{k})$ is the action spectral flux due to nonlinear wave–wave interactions; S_w represents action input by the wind; and D is the dissipation, primarily due to wave breaking. Since an explicit definition of D is not yet available, wave evolution models such as WAM rely on a tunable dissipation source term. As assessed by Banner and Young (1994), shortcomings in the dissipation source term lead to significant differences between predicted and observed spectral properties of fetch-limited waves.

In addition to the role in wave evolution, wave breaking has important dynamical roles in facilitating air–sea transfers. The breaking process acts to transfer momentum and energy from the waves to the upper ocean; Melville and Rapp (1985) showed that the momentum flux by breaking may be comparable to that transferred directly from the wind. As revealed in numerous observations of turbulent dissipation beneath surface waves, collated and presented by Agrawal et al. (1992) and further analyzed by Terray et al. (1996), the momentum flux from breaking waves provides an energy source for enhanced turbulence and mixing in the upper ocean with turbulent kinetic energy (TKE) dissipation rates that are one or two orders of magnitude above levels expected from a wall-bounded shear flow. Using laboratory data (Loewen and Melville 1991; Rapp and Melville 1990) and theoretical arguments (Phillips 1985), Melville (1994) concluded that the surface layer should be well mixed to a depth comparable to the breaking wave height with TKE dissipation rates in the range observed by Agrawal et al. (1992).

The entrainment of air is another important attribute of surface wave breaking. Using electrical conductivity sensors to map the air content, or void fraction distribution, under breaking laboratory waves of different amplitudes, Lamarre and Melville (1991) observed that void fractions of $>20\%$ were sustained for up to one-half wave period after breaking. Furthermore, the initial volume of entrained air was found to scale with the total energy dissipated by each breaking event; this led them to conclude that wave parameters obtained by remote sensing techniques may be used to quantify air entrainment and gas transfer in the field.

Whitecaps are a well-known surface signature of the breaking wave and air entrainment processes. Monahan and Lu (1990) classify whitecaps as either active (formed by the aerated spilling crest of a breaking wave in progress) or mature (the residual foam patch that remains after the active break). Combining several sets of observations, Wu (1992) notes a clear power-law dependence on wind forcing such that

$$W \sim u_*^3 \sim (C_{10}^{1/2} U_{10})^3 \sim U_{10}^{3.75}, \quad (2)$$

where W is the whitecap fraction, u_* is the friction velocity, and C_{10} is the 10-m-elevation atmospheric drag coefficient, assumed to scale with $U_{10}^{1/2}$. Wu points out that the relationships given by Eq. (2) are dynamically consistent since u_*^3 is proportional to the energy flux from the wind. Using modeled wave spectra, Cardone

(1970) found that W is better correlated with theoretical energy dissipation estimates than with wind speed alone. Furthermore, Kraan et al. (1996) recently observed a wave-age dependence of W, although with much scatter to their results.

Wave breaking and the bubble structures associated with breaking are now known to influence a variety of processes of global and operational significance (Banner and Donelan 1992; Melville 1996). For example, air–sea gas flux is enhanced by a factor of 2 or more above molecular diffusion in the open ocean when waves are breaking (Wallace and Wirick 1992; Farmer et al. 1993). In addition, Jessup et al. (1990) reported strong microwave returns from breaking waves in the field. They note that the contribution of breaking waves to the radar cross section increases approximately as u_*^3, in agreement with theoretical arguments by Phillips (1988). Furthermore, the bubbles entrained by breaking waves are found to be the dominant natural source of underwater ambient noise when winds are above the 3 m s^{-1} breaking threshold (Kerman 1988, 1993; Buckingham and Potter 1995). It is thought that ambient noise could be an indicator of air–sea gas transfer (Melville 1996). Finally, near-surface bubble populations are now known to be the dominant contributor to low-frequency ($\leq$1000 Hz) acoustic scatter and reverberation near the ocean surface (Ogden and Erskine 1994; McDaniel 1993).

In place of a detailed physical representation of breaking waves and the subsequent development of bubble clouds, empirical process models for air–sea gas flux, sonar and radar performance, etc., typically employ wind speed expressions to describe the wave-induced effects. Examples include the thin-film model for air–water gas transfer (Jähne 1990), which includes a wind-speed-dependent diffusion coefficient; the Wenz curves for ambient noise (Wenz 1962), which yield a power-law dependence of ambient noise on wind speed; and the Ogden–Erskine model for low-frequency acoustic backscatter (Ogden and Erskine 1994), which employs wind speed as the only environmental variable in a multiparameter fit to experimental data. The use of short-term averaged wind speed to describe wave-related processes will lead to prediction inaccuracies as the state of wind wave development at any given time represents an integrated effect of both the previous wind history and its spatial variability (Huang 1986).

Attempts have been made to augment or replace wind speed with wave parameters in air–sea process modeling. These have usually failed when bulk wave statistics were chosen; average wave parameters tend to smear the information from distinct wind sea and swell wave systems. Wallace and Wirick (1992), however, note a better correlation of mixed-layer oxygen saturation levels with wave height than with wind speed. Their results do not match the standard thin-film gas diffusion model but are more comparable to predictions from a model by Thorpe (1984) that include enhanced transfer by bubbles. The correlation between ambient noise A_N and various surface wave parameters was investigated by Felizardo and Melville (1995). They isolate wind sea spectra from full energy–frequency spectra by locating a spectral minimum between wind sea and swell peaks and then filtering the lower frequencies from the data. They note a high correlation between A_N and wind sea rms amplitude that was comparable to that between wind speed U and A_N. The correlation of A_N to various estimates of wave dissipation rate, obtained from the wind and wave observations using the separate ideas of Phillips (1985) and Hasselmann (1974), were also quite successful. These results, along with those obtained by Wallace and Wirick, suggest that properly chosen wave parameters can be used to augment or replace wind forcing parameters to improve the predictions of air–sea process models.

The primary objectives of the work reported here were to investigate wind sea growth and dissipation in the open ocean and to determine if wave parameters are more appropriate than wind speed parameters for estimation of wave breaking phenomena. These were accomplished using a spectral partitioning method for the isolation of distinct wind sea and swell wave components from directional wave spectra obtained from a heave, pitch, and roll buoy. Statistics generated from the wind sea partitions were employed to explore the influence of wind history and background swell on wave growth in the open ocean environment.

Furthermore, the equilibrium range theory of Phillips (1985) was employed to estimate the total rate of wave dissipation by breaking and to explore the relationships among wave dissipation, related air–sea parameters, and oceanic whitecap coverage. We believe the results have important implications for the use of surface wave parameters in air–sea process models.

2. Observations

Open ocean wind and wave observations were obtained during the Gulf of Alaska Surface Scatter and Air–Sea Interaction Experiment, conducted from 24 February through 1 March 1992, as part of the Critical Sea Test Program (Tyler 1992; Hanson and Erskine 1992; Hanson 1996). Located in the central Gulf of Alaska at 48°45′N, 150°00′W, the experiment was specifically designed to study the influence of the air–sea boundary zone on underwater acoustic scatter and reverberation at frequencies below 1000 Hz. Here we focus on the wind, wave, and whitecap observations made during this experiment. The collection and processing of these data, described elsewhere (Hanson 1996; Monahan and Wilson 1993), are briefly summarized below for completeness.

a. Atmospheric measurements

A MINIMET meteorological buoy (Coastal Climate Co.) was deployed by C.S.S. *John P. Tully* to obtain

wind speed and direction, air temperature, sea surface temperature, relative humidity, and barometric pressure measurements at 1-Hz resolution. The data were averaged over 30-min windows and input to a stability-dependent marine atmospheric boundary layer model (Hanson and White 1991; Smith 1988) to obtain estimates of vector-averaged wind velocity at a 10-m height (U_{10}) and wind friction velocity (u_*). Similar meteorological observations, obtained by a shipboard meteorological station mounted on R/V *Cory Chouest*, show excellent agreement with the MINIMET observations (Hanson et al. 1993).

b. Wave buoy data

Surface wave observations were obtained by a Datawell WAVEC buoy deployed from *John P. Tully*. The iterative eigenvector (IEV) method of Marsden and Juszko (1987) was employed by Juszko et al. (1995) to compute 236 half-hourly directional wave spectra over a 0.05–0.56 Hz band from the buoy heave, pitch, and roll time series. A data-adaptive technique, the IEV method has the advantage of exceptional peak resolution within multimodal spectra such as those obtained from the swell-dominated Gulf of Alaska. In robust comparisons with direct maximum likelihood (ML) and iterative maximum likelihood (IML) methods, using both simulated data and more than 350 real spectra, the IEV method produced low errors comparable to the IML method and was superior at producing narrower, more sharply defined peaks at all noise levels (Marsden and Juszko 1987).

A wave partitioning and swell tracking method (Hanson 1996) was employed to isolate wind sea from swell in the buoy observations. Based on an inverted catchment area approach (Hasselmann et al. 1994; Voorrips et al. 1997), wave partitioning is accomplished by dividing each directional wave spectrum into distinct subsets, or partitions, by defining partition boundaries as the minima between peaks. Recombining statistically similar peaks yields a set of individual partitions that represent the wave energy contributed from specific wind generation events. Peak separation and recombination criteria are tunable for a particular observation set; this leads to consistent results obtainable with different buoy platforms and spectral processing methods. We have applied this technique to several different observation sets originating from a variety of buoy types (Datawell, Seatec, and National Data Buoy Center platforms), and employing various processing techniques (IEV, ML, maximum entropy) with consistently good results (Hanson and White 1997; Kline and Hanson 1995). Wind sea peaks lie within the parabolic boundary defined by

$$c_p \leq 1.5U_{10}\cos\delta, \tag{3}$$

where δ is the minimum angle between the wind and the waves. The factor of 1.5 ensures that all possible wind sea peaks are included. All remaining partitions with energy are swell.

Spectral partitioning provides a preliminary isolation of spectral peaks that lie within the wind-forced spectral domain. During times of fluctuating winds, however, young swell components may also occupy this spectral region. Here the equilibrium range theory of Phillips (1985) is employed to identify the ''active'' portion of the wind sea spectrum directly involved with ''local'' energy transfers, including wave dissipation by breaking. For wind-generated gravity waves, Phillips argued for the existence of a spectral equilibrium range where the source terms for wind input (S_w), wave dissipation (D), and nonlinear wave–wave interactions ($S_{\rm nl}$) are in a state of statistical balance such that

$$S_w + S_{\rm nl} - D = 0.$$

Using theoretical arguments for $S_{\rm nl}$ and experimental evidence for S_w, Phillips derived an expression for the wave frequency spectrum in the equilibrium range:

$$S(\omega) = \alpha u_* g\omega^{-4}, \tag{4}$$

where α ranged from 0.06 to 0.11 in experimental data reviewed by Phillips. This range also fits with the observations reported here.

The concept of an equilibrium range is used to discriminate between actively generating wind sea spectral components, which should be maintained above a minimum threshold level set by $\alpha = 0.06$ in Eq. (4), and swell components, which are not maintained in local equilibrium and hence may fall below the energy threshold.

Indeed, examination of the Gulf of Alaska wind wave partitions indicates that active wind seas are typically separated from young swell by gaps in the spectrum where energy values fall below the $\alpha = 0.06$ threshold level. A typical case is depicted in Fig. 1. The original ''parent'' spectrum (dashed line) exhibits a dominant swell peak and a lesser wind sea peak. The wind wave spectrum isolated by the spectral partitioning process is depicted by a solid curve in Fig. 1. The actively generating wind sea components, isolated using the equilibrium range threshold criteria, are identified as that part of the solid curve with open circles. A lower-frequency peak, contained in the original wind wave partition, has been excluded by the $\alpha = 0.06$ threshold criterion and is regarded as young swell. This excluded peak has a wave age $c_p/U_{10} = 1.1$, which is slightly less than the $c_p/U_{10} = 1.2$ point of full development as determined by Pierson and Moskowitz (1964). This is understandable since winds were steadily increasing prior to the observation depicted in Fig. 1 and seas were most certainly duration limited.

Results of the wind sea isolation process appear in Fig. 2. Bulk significant wave heights H_s, as determined from the full original spectra prior to partitioning, are plotted with U_{10} in Fig. 2a. Although H_s depicts an increasing trend with U_{10}, there is much scatter in the

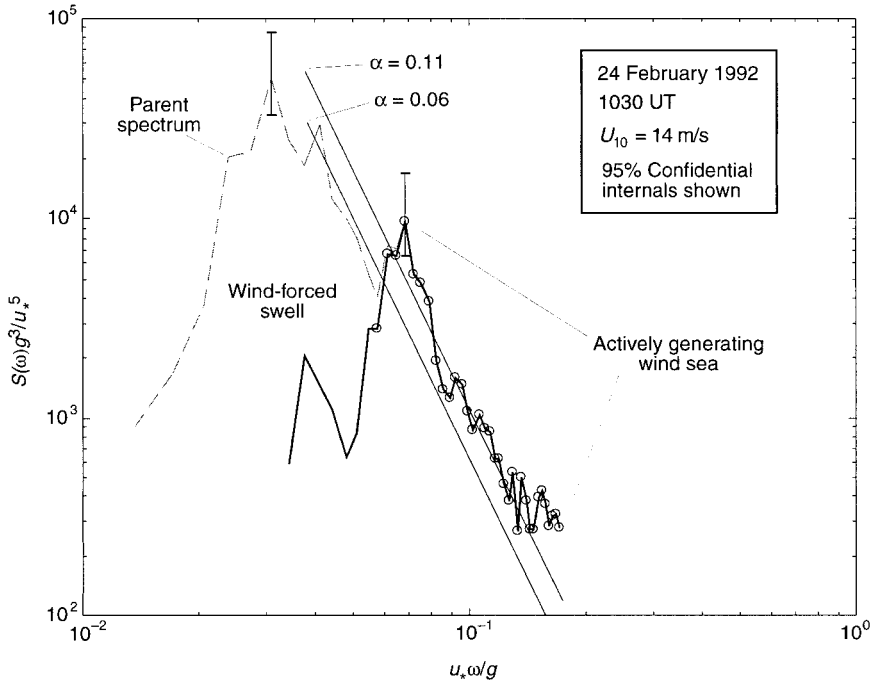

FIG. 1. Typical Gulf of Alaska wave spectrum (dimensionless) showing the full original parent spectrum (dashed line), partitioned wind wave spectrum (solid line), and actively generating wind sea with young swell components removed (open circles). Equilibrium range model representations for $\alpha = 0.06$ and 0.11 are included.

correlation. Furthermore, when wind speeds diminish to less than 5 m s^{-1}, wave heights of at least 2 m remain. These traits are due to the considerable amount of swell present in the Gulf of Alaska. These swells originated from storms up to 5000 km distant and, therefore, were not directly associated with the local wind forcing (Hanson 1996). The wind sea significant wave heights H_{ws}, derived from the active wind sea spectral subsets, are plotted with U_{10} in Fig. 2b. The wind sea significant wave heights exhibit nearly a U_{10}^2 dependence; this is in agreement with the JONSWAP results (Hasselmann et al. 1973). The scatter of H_{ws} values is principally attributed to wave age and wind history effects. These factors are further addressed in the following section.

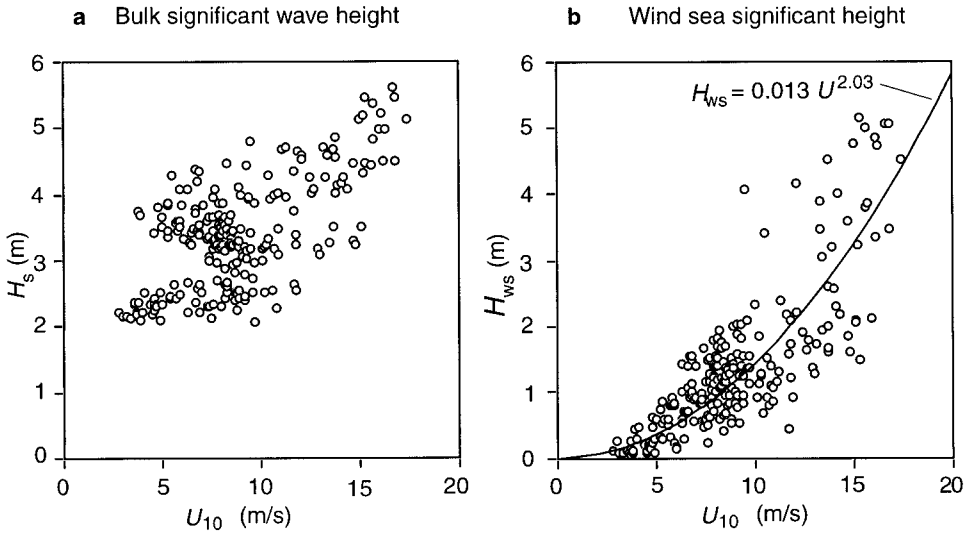

FIG. 2. Correlation of wind speed to significant wave heights as determined from (a) full original spectra and (b) active wind sea subsets. High values of H_s during low winds are a result of swell in the wave records. Swell removal results in a U^2 dependence of H_{ws} as observed during JONSWAP.

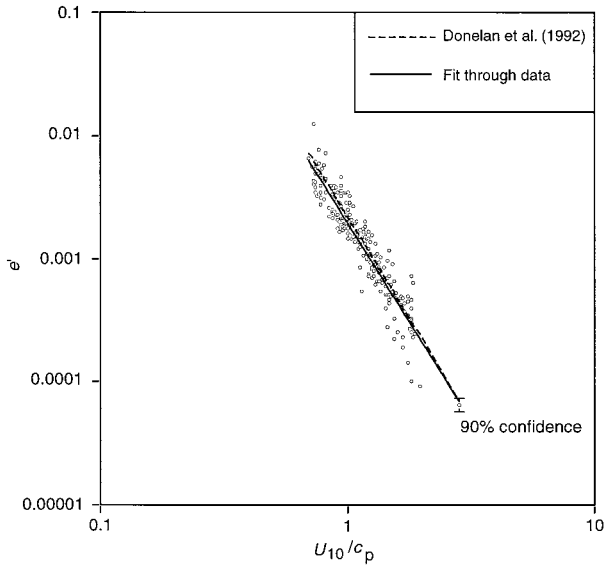

FIG. 3. Nondimensional energy of actively generating wind sea observations obtained with $U_{10} \geq 5.0$ m s^{-1}. Regressions through these data (solid line) and those of Donelan et al. (1992) (dashed line) are included.

c. Whitecap video observations

An additional estimate of breaking wave intensity was obtained by continuous video recordings of the sea surface during daylight hours using video camera systems mounted in heated instrument shelters on the sides of *John P. Tully* and *Cory Chouest* (Monahan and Wilson 1993). The video images were analyzed using an image processing technique to evaluate the fraction of the sea surface with Stage A (active spilling crest) whitecaps (Monahan 1993) during the experiment.

3. Wind sea growth in the open ocean

From comprehensive observations of wind wave growth on Lake St. Clair, Donelan et al. (1992) report a high correlation of nondimensional wave energy $e' = eg^2/U_c^4$ with inverse wave age U_c/c_p. For our analysis, U_{10} has been used in place of U_c since wave-induced motions of floating meteorological stations have been found to induce error into the directional resolution of attached wind sensors (Dugan 1991). Indeed, attempts to use U_c in these analyses resulted in poorer correlations. Furthermore, observations made with $U_{10} < 5.0$ m s^{-1} were dropped from the record because of the greater uncertainty in buoy measurements of small, high-frequency waves.

The Gulf of Alaska results, appearing in Fig. 3, depict a high correlation of wind sea energy to inverse wave age. The 90% confidence interval for these observations, estimated using the approach of Skafel and Donelan (1983), appears on the plot. A least squares regression curve on the plot is given by

$$e'_{ws} = 0.0020\left(\frac{U_{10}}{c_p}\right)^{-3.22}, \quad (5)$$

with a correlation of $r = 0.94$. Also included on Fig. 3 is a regression from the Lake St. Clair observations of Donelan et al. (1992):

$$e'_L = 0.0022\left(\frac{U_{10}}{c_p}\right)^{-3.3}, \quad (6)$$

where the L subscript is used to denote lake data. The open ocean observations are statistically identical with the Lake St. Clair results. This agreement is remarkable considering the drastic differences between the two sites: one a swell-dominated open ocean environment and the other a sheltered lake setting with no swell. From these results there is no directly discernible effect of swell on wind sea growth. There is, however, sufficient scatter beyond the 90% confidence limits to warrant additional investigation of these data. In the following sections we examine, first, the effect of wind history variability on wind sea growth and then look in greater detail at wind sea modification by swell.

a. Wind history effects

Since the response of the ocean surface to wind speed and direction changes is not instantaneous, it is likely that some of the remaining scatter in Fig. 3 is attributable to the recent wind history prior to each observation. Specifically, the mean rate at which wind speeds are rising or falling prior to each wave observation ought to determine, in addition to the current wind speed, the state of sea development. Indeed, it was noted by Toba et al. (1988) that the equilibrium range spectral level α becomes smaller for accelerating wind conditions and vice versa. To quantify the wind history conditions for each Gulf of Alaska wave observation, a 3-h averaging window was used to compute the mean wind speed $\overline{U}_{10}$. The mean rate of change or acceleration of the wind was then computed for each observation:

$$\overline{a}_U = \Delta\overline{U}_{10}/\Delta t, \quad (7)$$

where Δt represents a 15-min interval. A comparison of the U_{10}, $\overline{U}_{10}$, and $\overline{a}_U$ records from the Gulf of Alaska appears in Fig. 4.

The nondimensional wind sea energies observed during rising ($\overline{a}_U > 0.0002$ m s^{-2}) and falling ($\overline{a}_U < -0.0002$ m s^{-2}) wind conditions appear in Fig. 5 with separate symbols and regression lines for each. Again, observations made with $U_{10} < 5$ m s^{-1} are excluded from the analysis. A distinct grouping of the two observation sets indicates that wind seas under falling wind conditions are more developed both in energy content and location of the spectral peak. The latter is evident by the shift of falling wind observations to larger inverse wave ages. Although not shown (to preserve clarity), a

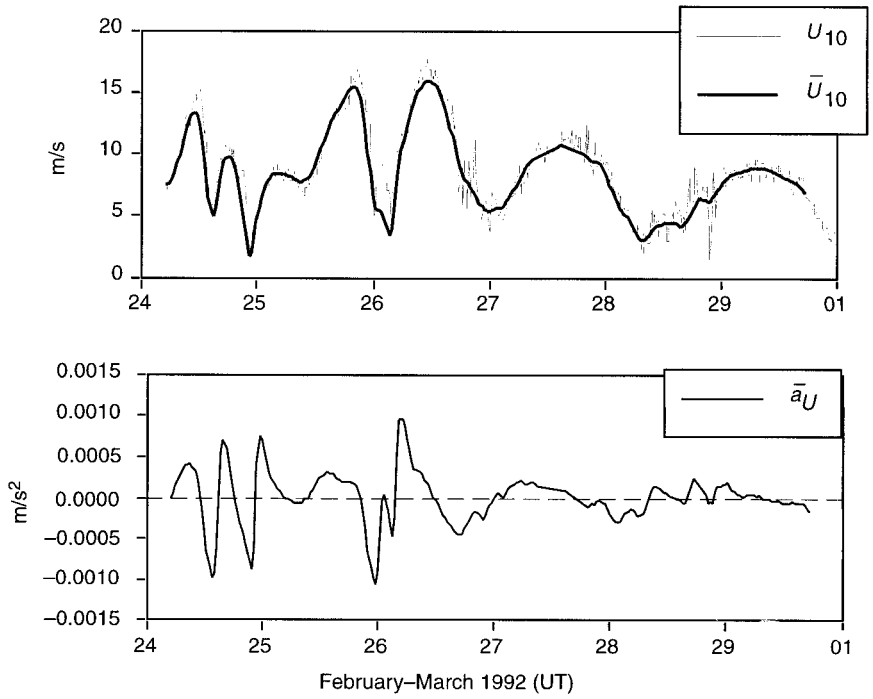

FIG. 4. Various wind parameters used in the evaluation of wind history effects: 15-min average wind (U_{10}), 3-h average wind ($\bar{U}_{10}$), and 3-h average wind acceleration ($\bar{a}_U$).

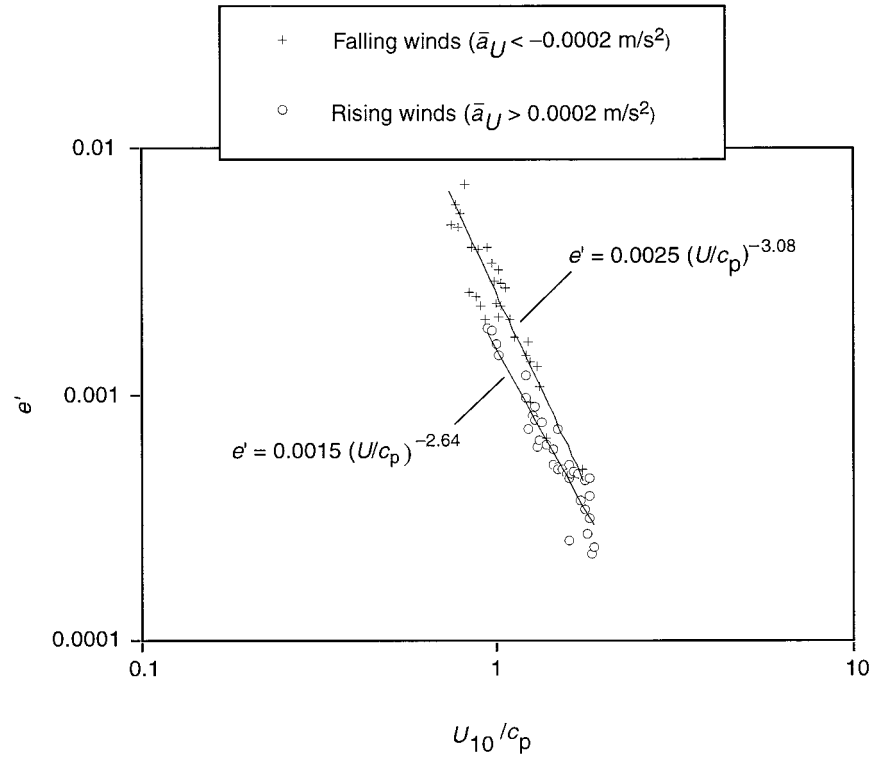

FIG. 5. Nondimensional wind energy in falling and rising wind conditions.

TABLE 2. Sorting of wave observations by swell conditions.

Wave category	Selection criteria	Number of observations
No swell	$\Psi_{s1} < 0.5\Psi_{ws}$	81
Aligned swell	$e_{ws} > 0$	
	$\Psi_{s2} < 0.5\Psi_{s1}$	42
	$0° \le \lvert\theta_{s-ws}\rvert \le 45°$	
Opposed swell	$e_{ws} > 0$	
	$\Psi_{s2} < 0.5\Psi_{s1}$	15
	$135° \le \lvert\theta_{s-ws}\rvert \le 180°$	
Confused sea	All other conditions	98

regression through a steady wind observation subset ($-5 \times 10^{-5} < \overline{a}_U < 5 \times 10^{-5}$) is given by

$$e'_{ws} = 0.0021\left(\frac{U_{10}}{c_p}\right)^{-2.73}, \quad (8)$$

which falls directly between the rising and falling wind regressions shown in Fig. 5. These results depict a trend of increasing energy with decreasing wind acceleration for observations at a given wave age and are in agreement with the findings of Toba et al. (1988). This important effect is ignored by air–sea process models that employ a short-term average wind speed forcing.

b. Interaction with swell

As discussed in the introduction, to date there has been little or no evidence that swells influence wind sea growth, over the range of frequencies observed by wave buoys, in the open ocean. It is clear that, at least for laboratory waves, the presence of long waves results in the attenuation of aligned wind waves. The mechanism for this process is as yet unresolved; the results from numerous laboratory and theoretical treatments are inconclusive and at times contradictory (Table 1). The agreement shown here between observations in the swell-dominated Gulf of Alaska and those from Lake St. Clair suggests that the relationship between eg^2/U^4 and U/c_p of natural wind waves is not affected by the presence of swell.

To more fully address the interaction between swell and wind sea in the Gulf of Alaska, the information assimilated through the wave spectral partitioning process was employed. To isolate specific swell conditions, the wave observations were sorted based on ratios between wind sea significant slope Ψ_{ws}, dominant swell partition significant slope Ψ_{s1}, the significant slope of the second largest swell partition Ψ_{s2}, and the angle θ_{s-ws} between the wind sea and dominant swell directions. Here the significant slope (Huang 1986)

$$\Psi = \frac{H_s}{\lambda_p} = \frac{\omega_p^2 H_s}{2\pi g} \quad (9)$$

is computed using the peak frequency (ω_p) and H_s statistics from the appropriate spectral partition. Four wave condition categories were formed as identified in Table 2. Most of the observations fall under the confused sea category, indicating the simultaneous existence of two or more swell systems with comparable steepness.

Nondimensional wind sea energy as a function of inverse wave age for the opposed swell and aligned swell categories (Table 2) appears in Fig. 6. Also appearing on the plot is the best-fit regression of the no-swell observations, given by

$$e' = 0.0022\left(\frac{U_{10}}{c_p}\right)^{-3.02}, \quad (10)$$

with a correlation of $r = 0.94$. The results suggest that the relationship of nondimensional wind sea energy to inverse wave age is independent of the presence of swell, regardless of the direction of swell propagation relative to the wind sea direction.

These results do not necessarily contradict the laboratory results from previous investigations. Chu et al. (1992) observed the interactions between statistically steady wind-generated waves and groups of longer waves of various slopes. During the interaction phase, they noted both a reduction of wind wave amplitudes by breaking near the long wave crests and a shortening of the wind waves due to straining by the wave orbital velocities of the group. The important point is that these two interaction effects are compensating, such that wind wave slope was essentially unchanged from its original value before the interaction. In terms of the nondimensionalization employed herein, swell interactions would be expected to decrease e' because of enhanced breaking while simultaneously decreasing the wavelength λ because of orbital straining. Hence, assuming that the deep water simplification

$$c_p = \left(\frac{g}{k}\right)^{1/2} = \left(\frac{g\lambda}{2\pi}\right)^{1/2}$$

holds for this scenario, a corresponding increase in U/c_p would occur. This simultaneous decrease of e' and increase of U/c_p suggests that the occurrence of swell would not change the dependence of e' on U/c_p.

4. Wave dissipation

a. Equilibrium range model

The equilibrium range theory of Phillips (1985) provides the necessary framework for obtaining estimates, from actual wave observations, of the total wave energy dissipation rate ε_t. By assuming a dependence of each term on the developing spectrum, Phillips employed theoretical and empirical arguments to derive the equilibrium range wave number and frequency spectral forms:

$$\Psi(\mathbf{k}) = \beta(\cos\theta)^p u_* g^{-1/2} k^{-7/2}, \quad (11)$$

$$S(\omega) = 4\beta I(p) u_* g \omega^{-4}, \quad (12)$$

where $I(p)$ is a spreading function given by

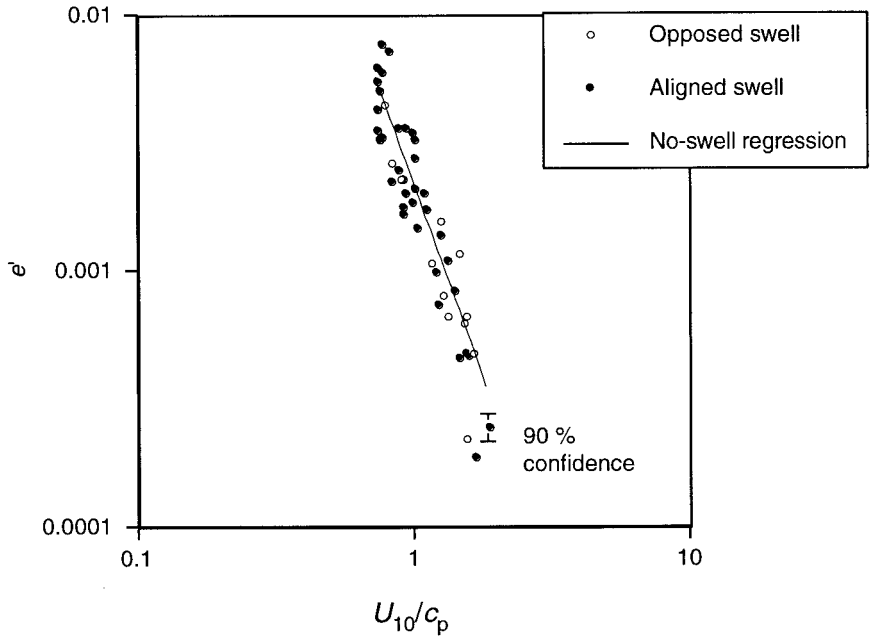

FIG. 6. Nondimensional wind sea energy during conditions of swell opposed with wind sea (open circles) and swell aligned with wind sea (solid circles). Although the no-swell observations are omitted for clarity, a regression through these observations is included on the plot.

$$I(p) = \int_{-(\pi/2)}^{\pi/2} (\cos\delta)^p \, d\delta, \tag{13}$$

and β is related to Toba's constant (α) and $I(p)$ by

$$\beta = \frac{\alpha}{4I(p)}. \tag{14}$$

The equilibrium range concepts allow for the expression of each source term as a function of the equilibrium range spectrum. The spectral rate of energy loss in the equilibrium range is given by

$$\varepsilon(\mathbf{k}) = \omega D(\mathbf{k}) = \gamma\beta^3(\cos\delta)^{3p}u_*^3k^{-2}. \tag{15}$$

This expression indicates that breaking waves provide energy for near-surface turbulence over the full range of scales in the equilibrium range. Equating the dissipation rate to the rate of energy input by the wind reveals

$$\gamma\beta^2 \approx m \approx 0.04, \tag{16}$$

and combining Eqs. (14) and (16),

$$\gamma \approx 0.04 \Big/ \left(\frac{\alpha}{4I(p)}\right)^2. \tag{17}$$

The equilibrium range ideas can be used to develop an expression for the total rate of wave dissipation ε_t in terms of a measured directional wave spectrum $S(\omega, \theta)$. First it is necessary to express the spectral dissipation rate [Eq. (15)] in terms of frequency. This transformation is given by (Phillips 1977, 1985)

$$\varepsilon(\omega) = 2\int_{-\pi/2}^{\pi/2} k\frac{dk}{d\omega}\varepsilon(k)\, d\delta\Big|_{k=\omega^2/g}. \tag{18}$$

Substituting Eq. (15) into the above and solving yields

$$\varepsilon(\omega) = 4\gamma\beta^3 I(3p)\frac{u_*^3}{\omega} \tag{19}$$

for $k = \omega^2/g$.

The spectral dissipation rate can be cast in terms of the equilibrium range spectrum by first solving equation (12) for u_* and then inserting this result into Eq. (19):

$$\varepsilon(\omega) = \frac{\gamma I(3p)}{16[I(p)]^3 g^3}\omega^{11}S(\omega)^3. \tag{20}$$

Assuming that the equilibrium range extends from ω_p to higher frequencies, integrating over this range and putting in the water density factor yields the dimensionally correct total rate of wave energy dissipation

$$\varepsilon_t = \frac{\rho_w\gamma I(3p)}{16[I(p)]^3 g^3}\int_{\omega_p} \omega^{11}S(\omega)^3 \, d\omega. \tag{21}$$

Felizardo and Melville (1995) use this expression to compare wave dissipation rate estimates with ambient sound signatures of breaking waves. They use wind sea frequency spectra, obtained by filtering out what was considered to be swell energy from observed wave frequency spectra, in place of $S(\omega)$ in Eq. (21), along with constant $I(p)$ spreading terms. Felizardo and Melville compare results of using Eq. (21) with those obtained using a dissipation expression proposed by Komen et

al. (1984). This alternate approach follows theoretical arguments of Hasselmann (1974) that spectral dissipation should approach a linear proportionality with $S(\omega)$ and exhibit a damping coefficient proportional to ω^2. In Felizardo and Melville's correlations of spectral dissipation rate with ambient noise levels, Eq. (21) performed at a level comparable to, if not slightly better than, the Komen et al. approach (see Fig. 19 in Felizardo and Melville 1995). Thus we will proceed with the development of Eq. (21), however noting the existence of an alternate method that has been shown to produce statistically similar results.

Perhaps the most significant limitation of the equilibrium range theory is the $I(p)$ directional spread factor defined by Eq. (13). This factor has its roots in the Plant (1982) wind input equation, which reasonably uses cos δ to obtain the component of wind stress that is in the direction of wave propagation. However, the use of this method to calculate $I(p)$ yields a spreading function that assumes a symmetrical wave spectrum developed through a hypothetical u_* stationarity. As directional distributions of wave spectra are now routinely measured, it is conceivable that the $I(p)$ terms of Eq. (21) could also be replaced with observational data.

A convenient directional spread indicator that has the same limits as cos δ, yet is derived from observations, is the normalized direction spectrum

$$S(\theta)_N = \frac{S(\theta)}{S(\theta_p)}, \tag{22}$$

where the wave direction spectrum in the equilibrium range is defined by

$$S(\theta) = \int_{\omega_p} S(\omega, \theta)\, d\omega \tag{23}$$

and $S(\theta_p)$ represents the equilibrium range peak. New spreading functions are defined as

$$I_1 = \int_{\theta_p-\pi/2}^{\theta_p+\pi/2} S(\theta)_N\, d\theta, \tag{24}$$

$$I_3 = \int_{\theta_p-\pi/2}^{\theta_p+\pi/2} [S(\theta)_N]^3\, d\theta. \tag{25}$$

Substitution of I_1 and I_3 in place of $I(p)$ and $I(3p)$, respectively, in Eq. (21) yields an estimate of the total rate of wave energy dissipation based on attributes of the directional wave spectrum:

$$\varepsilon_t = \frac{\rho_w \gamma I_3}{16 I_1^3 g^3} \int_{\omega_p} \omega^{11} S(\omega)^3\, d\omega, \tag{26}$$

with

$$\gamma = 0.04 \Big/ \left[\frac{\alpha}{4I_1}\right]^2. \tag{27}$$

b. Open ocean dissipation estimates

Directional wave spectra over the equilibrium range are required to satisfy the dissipation model assumption. The wave partitioning process resulted in the isolation of a wind-forced spectral domain as defined by the wave age criterion of Eq. (3) and the α threshold criterion (see Fig. 1). From these actively generating wind seas the equilibrium range $S_{ER}(\omega, \theta)$ is now defined as all spectral components that extend from the spectral peak to the high-frequency cutoff $f_c = 0.5$ Hz.

The total rate of wave energy dissipation (in units of kg s^{-3}) was estimated by applying Eqs. (24)–(27) to the Gulf of Alaska equilibrium-range directional spectra. These estimates represent the dissipation rate expected over the observed range of frequencies. The resulting Gulf of Alaska ε_t and I_1 records, along with wind speed and direction, appear in Fig. 7. As expected, dissipation rate is highest during the elevated wind events. As for the spreading parameter, trends in I_1 appear to be anticorrelated with wind speed. Lower I_1 values, indicative of directionally aligned seas, occur during the higher wind events when seas are more fully developed.

As Fig. 8 indicates, the dissipation rate estimates obtained from the wave spectra are fairly well correlated with wind speed. The data are fit by

$$\varepsilon_t = 4.28 \times 10^{-5} U_{10}^{3.74}, \tag{28}$$

with a correlation of $r = 0.82$. Also appearing on the figure are sample data points from Felizardo and Melville (1995), which from here on is referred to as FM95. The FM95 dissipation estimates fall within the range of scatter of the Gulf of Alaska estimates and exhibit a similar wind speed dependence. However, there is a nearly constant offset between the wind regressions of each observation set. Explanations for this offset are given in the discussion.

As demonstrated earlier, wind history effects can significantly influence wind sea growth (Fig. 5). Similarly, it is found that a significant portion of the scatter in the correlation of ε_t with U_{10} (Fig. 8) can be attributed to wind history trends not represented by the half-hour U_{10} averages. Figure 9 shows the correlation of mean (3-hourly) wind acceleration ($\overline{a}_U$), introduced earlier as a crude indicator of wind trend, with sorted ε_t observations in three specific wind speed bins. The wave dissipation rate exhibits a strong dependence on $\overline{a}_U$, with higher rates of dissipation when winds are falling. It is clear that wave dissipation estimates represent the integrated effect of the previous wind forcing history. This important information is lost when a short-term averaged wind speed is used to describe air–sea processes. This has significant implications for the use of wave parameters to augment wind speed in air–sea process modeling. An example of this, using whitecap observations from the Gulf of Alaska, is explored next.

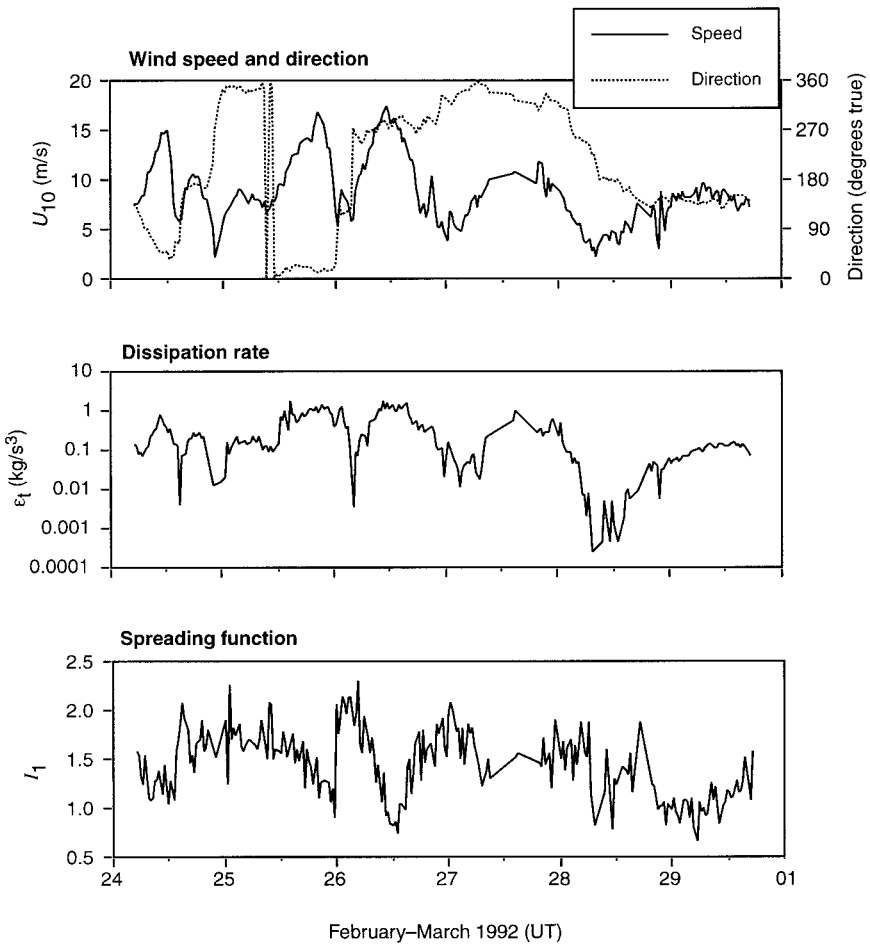

FIG. 7. Gulf of Alaska wind, wave dissipation rate, and spreading function records.

c. *Whitecaps*

Can wave dissipation rate estimates, obtained from surface wave observations, be used in place of wind speed to model ocean surface whitecaps? Cardone

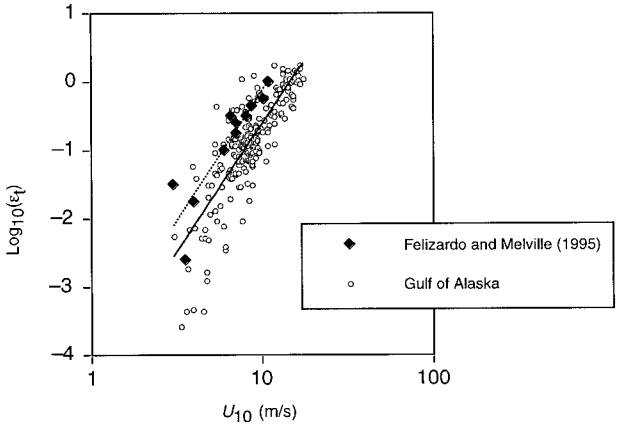

FIG. 8. Correlation of dissipation rate estimated from surface wave spectra with wind speed.

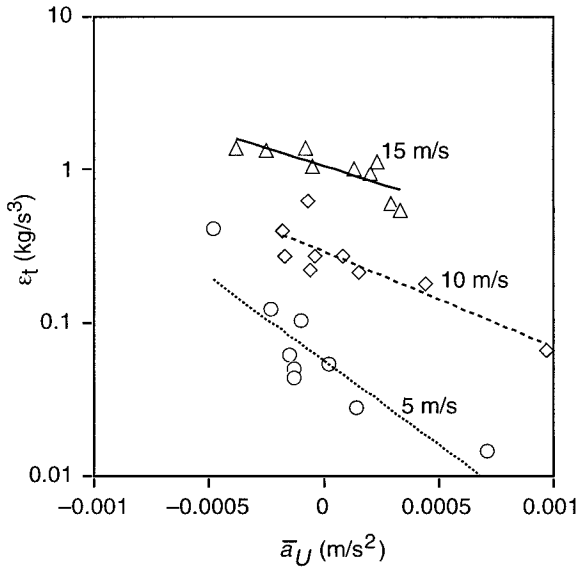

FIG. 9. Dependence of dissipation rate on mean wind acceleration at selected wind speeds.

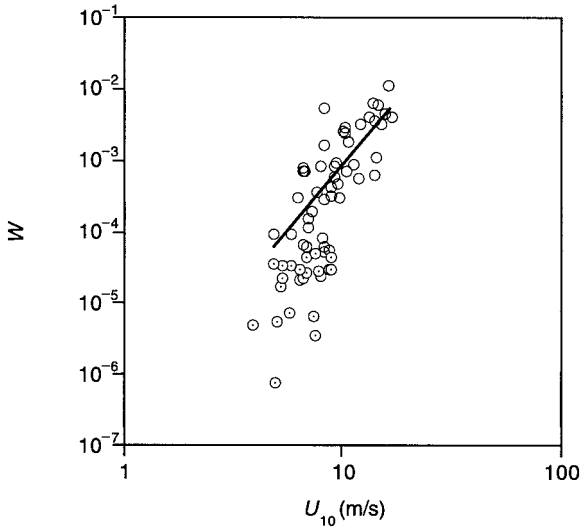

FIG. 10. Correlation of 30-min average whitecap fraction subset with wind speed. The power fit is computed over all $W > 5 \times 10^{-5}$. The points not included in this fit are identified by a dot in the circle center.

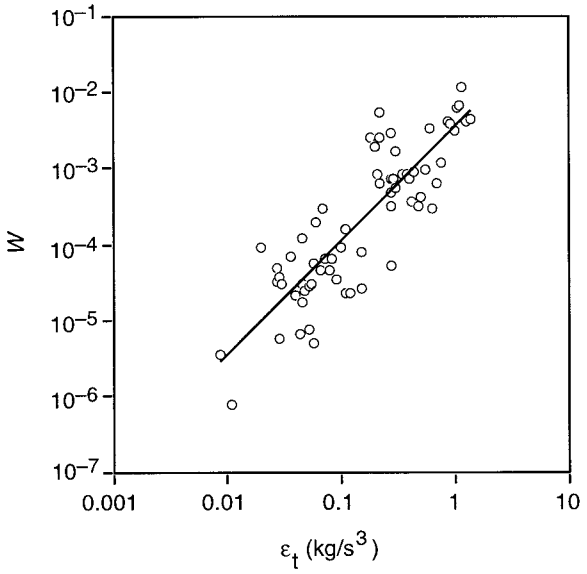

FIG. 11. Correlation of 30-min average whitecap fraction subset with dissipation rate.

(1970) observed that wave dissipation estimates, obtained from modeled wind seas, were better correlated with whitecap fraction estimates than with wind speed. Furthermore, the power-law fit of wind speed to wave dissipation rate, given by Eq. (28), additionally suggests that the answer to this question is yes. The U_{10} exponent of 3.74 is nearly identical to that noted by Wu (1992), and appearing in Eq. (2), for the correlation of whitecap fraction W to U_{10}. This agreement supports the laboratory findings of Lamarre and Melville (1991), who noted that the initial volume of air entrained by breaking is proportional to the energy dissipated by the wave. Whitecaps are breaking events marked by the generation of foam, and as long as they represent the dominant energy dissipation mechanism, one would expect that W would be directly proportional to ε_t such that

$$W \sim \varepsilon_t \sim u_*^3 \sim U^{3.75}. \tag{29}$$

The dependence of the Gulf of Alaska 30-min average W observations on U_{10} appears in Fig. 10. A power fit to *all* of these points gives

$$W = 3.66 \times 10^{-9} U_{10}^{5.16},$$

which is much steeper than the correlation (29) given by Wu. The observational data used by Wu exclude any values of $W < 5 \times 10^{-5}$, and if we also exclude these points, we obtain the best-fit solid line in Fig. 10 represented by

$$W = 2.04 \times 10^{-7} U_{10}^{3.61}, \tag{30}$$

with a correlation of $r = 0.72$. This is very close to Wu's result. It is evident from Fig. 10 that when $W < 5 \times 10^{-5}$, the scatter becomes very large and unsystematic, as each point represents an observation of only a few isolated whitecaps in the field of view. Variations in wind history, surface properties, and atmospheric stability may also contribute to the extreme variability in this range. Nevertheless, $\varepsilon_t \sim u_*^3$ should continue to hold even if, at low wind speeds, the breaking is not energetic enough to produce air entrainment and foam but is instead in the form of small-scale breaking and perhaps sporadic splashing with few bubbles entrained.

The use of the Gulf of Alaska wave dissipation rate estimates [Eqs. (26) and (27)] in place of wind speed improves the power-law description of whitecap fraction. The dependence of W on ε_t appears in Fig. 11. The whitecap power-law model

$$W = 3.4 \times 10^{-3} \varepsilon_t^{1.5} \tag{31}$$

fits all the observations with an improved correlation of $r = 0.86$. The scatter of W with ε_t is approximately two orders of magnitude less than that with U_{10}, and the "kink" in the W versus U_{10} distribution (Fig. 10) is removed by using ε_t. As will be further addressed in the discussion, the use of wave dissipation rate in place of wind speed removes the uncertainty caused by atmospheric forcing variability. The power of 1.5 on ε_t, rather than a power of unity as implied by (29), is likely a result of the fact that not all of the dissipation is represented by W. This is especially true with breaking at very small scales, which would likely produce surface manifestations too small for the detection capability of a ship-mounted whitecap video system.

5. Discussion

a. Wave dissipation estimates

Estimates of the total rate of wave energy dissipation by breaking surface waves in the Gulf of Alaska have

been conveniently obtained from wave buoy observations. On average, the Gulf of Alaska dissipation rates fell below those estimated from wave measurements off the coast of Oregon by FM95 (Fig. 8). Several factors could contribute to the increase in FM95 wave dissipation estimates over those obtained from the Gulf of Alaska, including 1) exclusion of dissipation in the spectral tail region, 2) the method employed to isolate the equilibrium range, and 3) geographic and seasonal trends in atmospheric forcing. Each of these will be discussed in turn.

1) DISSIPATION IN THE SPECTRAL TAIL REGION

FM95 used wire wave gauges to estimate wave frequency spectra; they present these estimates out to a cutoff frequency $f_c = 2.0$ Hz. If they estimated equilibrium range dissipation out to 2.0 Hz, then their dissipation estimates include more of the spectral tail region than those presented for the Gulf of Alaska ($f_c = 0.5$ Hz) and, hence, would be expected to be higher. But how much higher? To determine the importance of dissipation in the spectral tail, a simple relationship can be established assuming an ω^{-5} spectral falloff in this region as observed by Donelan et al. (1985). The total dissipation rate given in Eq. (26) can be expressed as

$$\varepsilon_t = P \int_{\omega_p} \omega^{11} S(\omega)^3 \, d\omega, \tag{32}$$

where P simply refers to the term in front of the integral. In line with Donelan et al. (1985), assume

$$S(\omega) \sim \omega^{-5} = C\omega^{-5}. \tag{33}$$

Substituting this into Eq. (32) and solving over the spectral tail region,

$$\tilde{\varepsilon}_t = P \int_{\omega_0} \omega^{11} (C\omega^{-5})^3 \, d\omega \tag{34}$$

$$= P \int_{\omega_0} C^3 \omega^{-4} \, d\omega \tag{35}$$

$$= \frac{1}{3} P C^3 \omega^{-3} \Big|_{\omega_0}^{\infty}, \tag{36}$$

where the integral has been evaluated from the radian cutoff frequency $\omega_0 = 2\pi f_c$ out to ∞. Since $C = S(\omega)\omega^5$, the total dissipation rate in the spectral tail can be expressed as a function of $S(\omega_0)$:

$$\tilde{\varepsilon}_t = \frac{1}{3} P \omega_0^{12} S^3(\omega_0). \tag{37}$$

Application of the tail dissipation correction factor to the Gulf of Alaska dissipation estimates results in just a few percent increase in $\log(\varepsilon_t)$. As the FM95 estimates are some 30%–40% higher than the Gulf of Alaska estimates, spectral dissipation in the tail region is not the primary cause of this offset.

2) ISOLATION OF THE EQUILIBRIUM RANGE

The theoretical concepts discussed earlier specify the equilibrium range to be a spectral region where the action flux due to wind input, nonlinear transfer, and wave dissipation are all in balance and proportional to each other. This refers to that portion of the spectrum where active exchanges are occurring and, hence, specifies the range over which the waves are breaking. Observations by Farmer and Vagle (1988) indicate a wide range of breaking scales, supporting the concept here that the equilibrium range extends from near the wind sea spectral peak out through the observed spectral tail.

FM95 isolated wind sea frequency spectra by locating a minimum between wind sea and swell peaks and filtering out spectral components at frequencies below this minimum. It appears that all spectral components above the minimum were considered to be wind sea. They defined the equilibrium range, for estimation of dissipation rate, as extending from the peak of the filtered wind seas to the end of the spectral tail at f_c. To this they applied a constant directional spreading of $I(p) = 2.4$.

As described, the Gulf of Alaska directional wind sea spectra were isolated using an automated spectral partitioning approach. An α-threshold test was employed to identify and remove young swell components that were found to exist within the wind-forced spectral domain. The premise here is that rapidly varying wind conditions can lead to a close spectral mix of wind sea and swell components and that these swell components, moving at speeds comparable to or slightly greater than the wind speed, are not actively involved in the equilibrium range exchanges. The removal of young swell components from isolated wind sea spectra would likely result in dissipation rate estimates that are lower than those obtained by the FM95 method. Although the constant $I(p)$ spectral spreading employed by FM95 would not contribute to a bias of the mean, it could result in an increased level of data scatter about the mean due to wind direction variability.

3) GEOGRAPHIC AND SEASONAL EFFECTS

As was demonstrated by Fig. 9, wind history trends factor prominently in the distribution of ε_t with U_{10}. The FM95 data were obtained during September at a location approximately 130 km off the Oregon coast. The atmospheric forcing trends, and the responses of the ocean to these trends, are expected to be different than those observed in the Gulf of Alaska during winter. Indeed, inspection of the FM95 wind records indicates that wind speeds varied on much slower timescales than those experienced in the Gulf of Alaska. Furthermore, the FM95 wind directions were reasonably steady during most of their experiment. As a result, the FM95 wave field, at a given wind speed, tended more toward full development and, hence, would be expected to ex-

hibit higher dissipation rates than were observed in the highly variable Gulf of Alaska environment.

b. Whitecap fraction correlations

Whitecap fraction has been shown to exhibit a better power-law relationship with wave dissipation rate than with wind speed (Figs. 10 and 11). The use of ε_t to describe W effectively removes the uncertainty due to wind trend that is present when U_{10} is used as the independent variable. Although surface wave parameters have been previously used to characterize the acoustics of breaking (Ding and Farmer 1994; FM95), the results reported here appear to be the first to show that observed surface wave parameters can be successfully used to characterize the whitecap signatures of wave breaking in the field.

What of the remaining scatter in W as a function of ε_t (Fig. 11)? Possibly, this variability is either dominated by measurement noise or represents limitations in the equilibrium range estimates of ε_t. There are, however, additional air–sea attributes that are thought to influence wave dissipation rates and air entrainment by breaking waves. These include, but are not limited to, atmospheric turbulence, atmospheric stability, water temperature, biological surfactants, directionality of the wave field, and the interaction with swell and surface currents. Of these effects, only the wave field directionality is addressed by the equilibrium range model.

6. Conclusions

A wave spectral partitioning approach has allowed an investigation of wind sea growth and dissipation in a swell-dominated open ocean environment. When scaled by eg^2/U^4, Gulf of Alaska wind seas exhibit the same functional dependence on inverse wave age U/c_p that was observed in a relatively benign lake setting by Donelan et al. (1992). It is concluded that the chosen scaling compensates for wind sea modification by swell; a decrease of eg^2/U^4 through swell interactions is accompanied by a compensating increase of U/c_p. This finding is consistent with the laboratory results of Chu et al. (1992) that show wind sea slope is preserved during interactions between wind sea and swell.

Using the 3-h average wind acceleration as a crude indicator of wind trend, it was found that the dependence of eg^2/U^4 on U/c_p is significantly influenced by wind history. At a given wave age, wind seas are more developed during falling winds due to the recent history of high winds, and they are less developed during rising winds for the opposite reason. This effect is not accounted for in empirical process models for air–sea gas flux (Jähne 1990), acoustic reverberation (Ogden and Erskine 1994), and ambient noise (Wenz 1962; Cato et al. 1995). It is likely that accounting for wind history effects would improve the accuracy of these models.

The total rate of wave energy dissipation (ε_t) was estimated from the Gulf of Alaska wind sea partitions using concepts from the Phillips (1985) equilibrium range theory [Eq. (24)–(27)]. Equilibrium ranges of directional wave spectra were isolated using a wave-age-dependent partitioning approach with an α-threshold criterion for the removal of young swell components near the wind sea peak. Furthermore, the $I(p)$ spreading functions in the Phillips theory have been replaced by directional spread indicators obtained from the wave observations.

Dissipation estimates obtained with this approach show a similar dependence on wind speed as reported by FM95. Furthermore, whitecap fraction estimates from ship-board video records obtained during the Gulf of Alaska experiment were used to evaluate power-law descriptions of whitecaps using wind speed and wave dissipation rate. Replacing wind speed with ε_t in the standard power-law description of whitecap fraction W resulted in a new proportionality,

$$W \propto \varepsilon_t^{1.5}, \tag{38}$$

that reduces the scatter of W about the independent variable by 2 to 3 orders of magnitude. These improvements result primarily from the removal of wind trend effects that add uncertainty to wind speed relationships. These open ocean results support the laboratory findings of Lamarre and Melville (1991); those authors observed a proportionality between the energy dissipated by breaking and the initial amount of air entrained. The successful description of whitecaps by our dissipation rate estimates lends credibility to the equilibrium range theory as a viable approach to modeling air–sea exchanges.

Remote sensing techniques, wave buoy arrays, and regional wave modeling efforts are continually being refined so that soon high-quality directional wave spectra will be routinely available on a global scale (Beal 1991). It is conceivable that air–sea process models for such mechanisms as gas flux, radar backscatter, underwater ambient noise, and near-surface acoustic reverberation will soon experience significant improvements due to the use of surface wave spectral parameters in place of external forcing parameters. Since wave-related processes are dynamically linked to intrinsic properties of the wave field (not necessarily to properties of the external forcing on the waves from winds, currents, bathymetry, etc.), use of wave parameters should improve model performance.

Acknowledgments. We are grateful to the many individuals who contributed to the logistics, acquisition, and processing of the field data. In particular, wave spectra were provided by Richard F. Marsden, whitecap video observations were provided by Ed Monahan, and meteorological observations were obtained by Larry White. We wish to thank Hans Graber for insightful discussions on wind–wave dynamics and Ken Melville for suggesting the wave dissipation calculations. We

thank the reviewers for their careful and helpful assessments. This work was supported by the Office of Naval Research (Code 321OA) under Grant N00014-97-1-0075. Additional support for manuscript preparation came from a Johns Hopkins University Applied Physics Laboratory Janney Fellowship Award.

REFERENCES

Agrawal, Y. C., E. A. Terray, M. A. Donelan, P. A. Hwang, A. J. Williams III, W. M. Drennan, and Coauthors 1992: Enhanced dissipation of kinetic energy beneath surface waves. *Nature,* **359,** 219–220.

Banner, M. L., and M. A. Donelan, 1992: The physical consequences of wave breaking in deep water. *Breaking Waves.* M. L. Banner and R. H. J. Grimshaw, Eds., Springer-Verlag, 3–20.

——, and I. R. Young, 1994: Modeling spectral dissipation in the evolution of wind waves, Part I: Assessment of existing model performance. *J. Phys. Oceanogr.,* **24,** 1550–1571.

Beal, R. C., Ed., 1991: *Directional Ocean Wave Spectra.* The Johns Hopkins Studies in Earth and Space Sciences, The Johns Hopkins University Press, 218 pp.

Buckingham, M. J., and J. R. Potter, Eds., 1995: *Sea Surface Sound '94.* World Scientific, 494 pp.

Cardone, V. J., 1970: *Specification of the Wind Distribution in the Marine Boundary Layer for Wave Forecasting.* New York University, 131 pp.

Cato, D. H., S. Tavener, and I. S. F. Jones, 1995: Ambient noise dependence on local and regional wind speeds. *Sea Surface Sound '94.* M. J. Buckingham and J. R. Potter, Eds., World Scientific, 95–111.

Chu, J. S., S. R. Long, and O. M. Phillips, 1992: Measurements of the interaction of wave groups with shorter wind-generated waves. *J. Fluid Mech.,* **245,** 191–210.

Cox, C. S., 1958. Measurements of slopes of high-frequency wind waves. *J. Mar. Res.,* **16,** 199–225.

Ding, L., and D. M. Farmer, 1994: Observations of breaking surface wave statistics. *J. Phys. Oceanogr.,* **24,** 1368–1387.

Dobson, F., W. Perrie, and B. Toulany, 1988: On the deep-water fetch laws for wind-generated surface gravity waves. *Atmos.-Ocean,* **27**(1), 210–236.

Donelan, M. A., 1987: The effect of swell on the growth of wind waves. *Johns Hopkins APL Tech. Dig.,* **8** (1), 18–23.

——, J. Hamilton, and W. H. Hui, 1985: Directional spectra of wind-generated waves. *Philos. Trans. Roy. Soc. London,* **315A,** 509–562.

——, M. Skafel, H. Graber, P. Liu, D. Schwab, and S. Venkatesh, 1992: On the growth rate of wind-generated waves. *Atmos.-Ocean,* **30** (3), 457–478.

Dugan, J. P., 1991: Decontamination of wind measurements from buoys subject to motions in a seaway. *J. Atmos. Oceanic Technol.,* **8,** 85–95.

Farmer, D. M., and S. Vagle, 1988: On the determination of breaking surface wave distributions using ambient sound. *J. Geophys. Res.,* **93** (C4), 3591–3600.

——, C. L. McNeil, and B. D. Johnson, 1993: Evidence for the importance of bubbles in increasing air–sea gas flux. *Nature,* **361,** 620–623.

Felizardo, F. C., and W. K. Melville, 1995: Correlations between ambient noise and the ocean surface wave field. *J. Phys. Oceanogr.,* **25,** 513–532.

Hanson, J. L., 1996: Wind sea growth and swell evolution in the Gulf of Alaska. Ph.D. Dissertation, The Johns Hopkins University, 151 pp.

——, and L. H. White, 1991: Assessment of the air–sea boundary zone during critical sea test 4. The Johns Hopkins University Applied Physics Laboratory Tech. Rep. STD-R-1978, 116 pp.

——, and F. T. Erskine, 1992: An experiment to study the influence of the air–sea boundary zone on underwater acoustic reverberation. *Proc. MTS '92,* Washington, DC, Marine Technology Society, 835–847.

——, ——, and M. Kennelly, 1993: Air–sea and upper ocean dynamics during CST-7 phase 2. The Johns Hopkins University Applied Physics Laboratory Tech. Rep. STD-R-2281, 74 pp.

Hasselmann, K., 1974: On the spectral dissipation of ocean waves due to whitecapping. *Bound.-Layer Meteor.,* **126,** 507–127.

——, T. P. Barnett, E. Bouws, H. Carlson, D. E. Cartwright, K. Enke, and Coauthors 1973: Measurements of wind–wave growth and decay during the Joint North Sea Wave Project (JONSWAP). *Deutsche Hydrographische Zeitschrift, Reihe A,* **8** (22), 1–95.

Hasselmann, S., K. Hasselmann, and C. Bruning, 1994: Extraction of wave spectra from SAR image spectra. *Dynamics and Modelling of Ocean Waves,* Cambridge University Press, 532 pp.

Hatori, M., M. Tokuda, and Y. Toba, 1981: Experimental study on strong interactions between regular waves and wind waves—I. *J. Oceanogr. Soc. Japan,* **37,** 111–119.

Huang, N. E., 1986: An estimate of the influence of breaking waves on the dynamics of the upper ocean. *Wave Dynamics and Radio Probing of the Ocean Surface,* O. M. Phillips and K. Hasselmann, Eds., Plenum Press, 295–313.

Jähne, B., 1990: New experimental results on the parameters influencing air–sea gas exchange. *Proc. on Air–Water Mass Transfer, Second Int. Symp.,* Minneapolis, MN, ASCE, 244–256.

Jessup, A. T., W. C. Keller, and W. K. Melville, 1990: Measurements of sea spikes in microwave backscatter at moderate incidence. *J. Geophys. Res.,* **95,** 9679–9688.

Juszko, B.-A., R. F. Marsden, and S. R. Waddell, 1995: Wind stress from wave slopes using Phillips equilibrium theory. *J. Phys. Oceanogr.,* **25,** 185–203.

Kerman, B. R., Ed., 1988: *Natural Mechanisms of Surface Generated Noise in the Ocean: Sea Surface Sound.* Kluwer Academic Publishers, 639 pp.

——, Ed., 1993: *Natural Physical Sources of Underwater Sound: Sea Surface Sound.* 2d ed. Kluwer Academic Publishers, 750 pp.

Kitaigorodskii, S. A., 1962: Applications of the theory of similarity to the analysis of wind-generated gravity waves. *Bull. Acad. Sci. USSR, Geophys. Ser.,* **1,** 105–117.

Kline, S. A., and J. L. Hanson, 1995. Wave identification and tracking system. Technical Report STD-R-2436, The Johns Hopkins University Applied Physics Laboratory Tech. Rep. STD-R-2436, 40 pp.

Komen, G. J., S. Hasselmann, and K. Hasselmann, 1984. On the existence of a fully developed wind-sea spectrum. *J. Phys. Oceanogr.,* **14,** 1271–1285.

——, L. Cavaleri, M. Donelan, K. Hasselmann, S. Hasselmann, and P. A. E. M. Janssen, 1994: *Dynamics and Modeling of Ocean Waves.* Cambridge University Press, 532 pp.

Kraan, C., W. A. Oost, and P. A. E. M. Janssen, 1996: Wave energy dissipation by whitecaps. *J. Atmos. Oceanic Technol.,* **13,** 262–267.

Lamarre, E., and W. K. Melville, 1991: Air entrainment and dissipation in breaking waves. *Nature,* **351,** 469–472.

Loewen, M. R., and W. K. Melville, 1991: Microwave backscatter and acoustic radiation from breaking waves. *J. Fluid Mech.,* **224,** 601–623.

Longuet-Higgens, M. S., and R. W. Stewart, 1960: Changes in the form of short gravity waves on long waves and tidal currents. *J. Fluid Mech.,* **8,** (Part 4), 565–583.

Marsden, R. F., and B.-A. Juszko, 1987: An eigenvector method for the calculation of directional spectra from heave, pitch and roll buoy data. *J. Phys. Oceanogr.,* **17,** 2157–2167.

McDaniel, S. T., 1993: Sea surface reverberation: A review. *J. Acoust. Soc. Amer.,* **94** (4), 1905–1922.

Melville, W. K., 1994: Energy dissipation by breaking waves. *J. Phys. Oceanogr.,* **24,** 2041–2049.

——, 1996: The role of surface-wave breaking in air–sea interaction. *Ann. Rev. Fluid Mech.,* **28,** 279–321.

——, and R. J. Rapp, 1985: Momentum flux in breaking waves. *Nature,* **317,** 514–516.
Mitsuyasu, H., 1966: Interactions between water waves and winds (I). *Rep. Res. Inst. Appl. Mech. Kyushu Univ.,* **14,** 67–88.
——, 1992: Wave breaking in the presence of wind drift and opposed swell. *Breaking Waves,* M. L. Banner and R. H. J. Grimshaw, Eds., Springer-Verlag, 147–153.
Monahan, E. C., 1993: Occurrence and evolution of acoustically relevant sub-surface bubble plumes and their associated, remotely monitorable, surface whitecaps. *Natural Physical Source of Underwater Sound: Sea Surface Sound.* 2d ed. Kluwer Academic 503–517.
——, and M. Lu, 1990: Acoustically relevant bubble assemblages and their dependence on meteorological parameters. *IEEE J. Oceanic Eng.,* **15** (4), 340–349.
——, and M. Wilson, 1993: Whitecap measurements. Critical Sea Test 7, Phase 2: Principal investigators' results. The Johns Hopkins University Applied Physics Laboratory Tech. Rep. STD-R-2258, F. T. Erskine and J. L. Hanson, Eds., 808 pp.
Ogden, P. M., and F. T. Erskine, 1994: Surface and volume scattering measurements using broadband explosive charges in the Critical Sea Test 7 experiment. *J. Acoust. Soc. Amer.,* **96** (5), 2908–2920.
Phillips, O. M., 1958: The equilibrium range in the spectrum of wind-generated waves. *J. Fluid Mech.,* **4,** 426–434.
——, 1977: *Dynamics of the Upper Ocean.* Cambridge University Press, 236 pp.
——, 1985: Spectral and statistical properties of the equilibrium range in wind-generated gravity waves. *J. Fluid Mech.,* **156,** 505–531.
——, 1988: Radar returns from the sea surface—Bragg scattering and breaking waves. *J. Phys. Oceanogr.,* **18,** 1065–1074.
——, and M. L. Banner, 1974: Wave breaking in the presence of wind drift and swell. *J. Fluid Mech.,* **66** (Part 4), 625–640.
Pierson, W. J., and L. Moskowitz, 1964: A proposed spectral form for fully developed wind seas based on the similarity theory of S. A. Kitaigorodskii. *J. Geophys. Res.,* **69** (24), 5181–5190.
Plant, W. J., 1982: A relationship between wind stress and wave slope. *J. Geophys. Res.,* **87** (C3), 1961–1967.
——, and J. W. Wright, 1977: Growth and equilibrium of short gravity waves in a wind-wave tank. *J. Fluid Mech.,* **82,** 767–793.
Rapp, R. J., and W. K. Melville, 1990: Laboratory measurements of deep-water breaking waves. *Philos. Trans. Roy. Soc. London,* **331A,** 735–800.
Skafel, M. G., and M. A. Donelan, 1983: Performance of the CCIW wave direction buoy at ARSLOE. *IEEE J. Oceanic Eng.,* **OE-8** (4), 221–225.
Smith, S. D., 1988: Coefficients for sea surface wind stress, heat flux, and wind profiles as a function of wind speed and temperature. *J. Geophys. Res.,* **93,** 15 467–15 472.
——, 1990: Modulation of short wind waves by long waves. *Surface Waves and Fluxes,* G. L. Geerhaert and W. J. Plants, Eds., Kluwer Academic, 247–284.
Terray, E. A., and Coauthors, 1996: Estimates of kinetic energy dissipation under breaking waves. *J. Phys. Oceanogr.,* **26,** 792–807.
Thorpe, S. A., 1984: The effect of Langmuir circulation on the distribution of submerged bubbles caused by breaking wind waves. *J. Fluid Mech.,* **142,** 151–170.
Toba, Y., K. Okada, and I. Jones, 1988: The response of wind–wave spectra to changing winds. Part I: Increasing winds. *J. Phys. Oceanogr.,* **18,** 1231–1240.
Tyler, G. D., 1992: The emergence of low-frequency active acoustics as a critical antisubmarine warfare technology. *Johns Hopkins APL Tech. Dig.,* **13** (1), 145–159.
Voorrips, A. C., V. K. Makin, and S. Hasselmann, 1997: Assimilation of wave spectra from pitch-and-roll buoys in a North Sea wave model. *J. Geophys. Res.,* **102** (C3), 5829–5849.
Wallace, D. W. R., and C. D. Wirick, 1992: Large air–sea gas fluxes associated with breaking waves. *Nature,* **356,** 694–696.
Wenz, G. M., 1962: Acoustic ambient noise in the ocean: Spectra and sources. *J. Acoust. Soc. Amer.,* **34,** 1936–1956.
Wright, J. W., 1976: The wind drift and wave breaking. *J. Phys. Oceanogr.,* **6,** 402–405.
Wu, J., 1992: Individual characteristics of whitecaps and volumetric description of bubbles. *IEEE J. Oceanic Eng.,* **17** (1), 150–158.